UDC 621.314

DOI: 10.20535/2523-4455.mea.291803

Generation of Anisotropic Cloud Cover

V. I. Martyniuk[f], 0000-0003-0882-5114
V. Ya. Zhuikov[s], 0000-0002-3338-2426
National Technical University of Ukraine "Igor Sikorsky Kyiv Polytechnic Institute" 00syn5v21
Kyiv, Ukraine

***Abstract*—This paper introduces an advanced mathematical model for generating and analyzing cloud cover images, specifically designed to enhance photovoltaic (PV) partial shading studies. The model development involved a detailed analysis of real cloud cover images, with a particular emphasis on capturing their anisotropic spectral characteristics. This was achieved through a combination of spectral analysis and advanced image processing techniques. The research methodologically focused on developing a four-parameter model to accurately represent cloud formations' spectral properties. Key parameters were identified and fine-tuned to match the real cloud formations' characteristics. This involved analyzing the magnitude and phase spectra of the cloud covers and fitting them to a model capable of replicating these properties accurately. A significant part of the research was dedicated to formulating a novel phase spectrum generation technique. This technique was specifically designed to control the degree of similarity between the synthesized and original images, thereby ensuring the model's effectiveness in various simulation scenarios. The process involved manipulating the phase information of cloud cover images while maintaining their high-frequency components to enhance the detail and realism of the synthesized images. The model's accuracy in replicating cloud cover features was tested against traditional spectral synthesis methods. This comparative analysis involved generating cloud cover images using the developed model and established methods, then comparing these images to the original cloud covers in terms of visual similarity and approximation error. Additionally, the model was utilized to generate pseudo-random cloud cover images by varying the phase spectrum parameters. This process ensured that the generated images, while being random, adhered to the spectral characteristics of the original cloud covers. The research methodology also involved a detailed examination of the images' key characteristics, such as direction, length, and density, to ensure fidelity to the original samples. In summary, this paper details an approach to cloud cover image synthesis, with a focus on the accuracy of spectral properties and the development of an algorithm of model parameters estimation. The research highlights the use of advanced spectral analysis and image processing techniques in deriving key model parameters, leading to a significant advancement in cloud imaging for solar energy applications.**

Keywords — spectral image synthesis; partial shading; cloud cover modeling; image approximation accuracy; spectral anisotropy; frequency response analysis; phase spectrum generation

I. Introduction

Year after year, electricity demand grows by 1.5-5% [1], and installing new generation capacities based on renewable energy sources (RES) is a promising and often indispensable method of meeting these increasing needs [2, 3]. Predictions suggest that by 2025, these demands will be fulfilled primarily by low-emission sources, predominantly through RES [4, 5]. Besides mitigating environmental impact, RES usage offers several other benefits, including decentralization and reduced electricity transmission losses, among others. In addition, RES are well aligned with the concept of distributed electricity generation. Despite this, a significant drawback of the use of RES is the variability and dependence of the output power on weather conditions [6].

Ukraine aligns with global trends by integrating RES into its energy system, as reflected in its energy strategy. This strategy underscores the importance of decarbonization and the utilization of RES in the energy sector [7]. According to approximate estimates, the technically achievable annual RES potential without taking into account hydropower of Ukraine is about 370 TWh [8, 9].

Among all renewable sources, solar energy has a special role. Over the last decade, considerable progress has been made in the technology of manufacturing solar panels, which has made them widely available and cost-effective [10, 11]. In addition, solar modules do not have moving parts and during their operation do not create noise and vibration pollution in comparison with wind energy. Coupled with supportive government policies, these factors have led to a substantial rise in the number of low-power autonomous solar power plants, primarily for private household use. That is why in Ukraine in 2021 the share of solar electricity was about 56% among other RES [9].

When operating a solar power plant, the panels receive different amounts of solar radiation [12]. This phenomenon is called the partial shading effect. The reasons for its occurrence can be various factors, but the most significant is the presence of cloud cover. In addition to reducing the output power, partial shading

DOI: 10.20535/2523-4455.mea.291803

can cause overheating and damage to individual elements of the solar panel [13, 14]. In this regard, a lot of research is being conducted to determine ways to minimize or eliminate the negative impact of the partial shading effect while simultaneously maximizing power extraction [15]. To check the effectiveness of these methods, a mathematical model of the cloud cover is needed, which will accurately reproduce the operation of the array of solar panels in conditions of partial shading.

The aim of this work is to develop a cloud cover simulation model that accurately replicates real-life conditions of partial shading and allows to maximize power output of solar panel array.

II. METHODS

A. Cloud optical thickness and 1/f noise

To quantify the impact of cloud cover on solar radiation received per unit area of a solar panel, the optical thickness of the cloud cover is used, determined as follows [16]:

$$\tau = \ln\frac{E_{e,i}}{E_{e,t}} = T,$$

where $E_{e,i}$ – illuminance of incident sunlight, $E_{e,t}$ – illuminance of transmitted through the medium sunlight, T – medium transmittance.

In practice, τ is measured experimentally by employing ground-based equipment, satellites, or a combination of these methods [17–19]. The disadvantage of using experimentally obtained data is the low frequency of measurements, which does not allow simulating the operation of an array of solar panels (SP) in real time. Consequently, an approach to cloud cover generation using a mathematical model that delineates the optical thickness of the cloud cover has gained popularity [20, 21].

Like most natural processes, the image of cloud cover has a characteristic of power spectral density (PSD), which is described by the following distribution law [22]:

$$S(f) \approx \frac{c}{f^{\alpha m}}, \qquad (1)$$

where m – dimension of space, $f = \sqrt{\sum_{i=1}^{m} f_i^2}$ – norm of the m-dimensional frequency vector $(f_1,\ldots,f_m)$, f_i – the frequency component along the i-th axis, α – fade coefficient, which defines the color of the process (noise), c – some coefficient.

In the discrete scenario, the PSD distribution law for noise follows the same description as in the continuous case (1).

Owing to the nature of its magnitude spectrum, this process is referred to $1/f$ noise. Similar processes are found in electronics [23], biology [24] and many other areas of human activity. In this regard, many studies have been conducted to analyze their nature, as well as to create a mathematical model [25].

The concept of noise is quite often used instead of the terms random process or signal, therefore, in further explanations, these definitions will be considered interchangeable.

For the sake of simplification, we introduce the definition of the term “noise” as a random process with the following properties:

1. Stationarity – absence of dependence of statistical parameters of this process (such as average value and variance) on time. This simplifies the analysis because the properties of the process remain constant.
2. The normal distribution law – at any moment in time, the process corresponds to a normal distribution, which is characterized by an average value and a standard deviation.
3. Spectrum range limitation – defined as noise having non-zero spectrum components exclusively within a specific frequency range or bandwidth. In many real-world scenarios, such limitations are observed where noise occurs within certain frequency ranges
4. Ability to control the PSD. The power spectrum of a signal reflects how its energy is distributed among different frequencies. By controlling the power spectrum, it is possible to control the energy distribution over the different frequency components of the noise. This can be important for reproducing the properties of real processes and phenomena. Such property can be achieved directly or by summing independent normalized noises.

The direct control of the noise spectrum significantly enhances its quality. Among the various cloud cover generation methods, the spectral synthesis method and its derivatives are notable for allowing spectrum control [26, 27].

B. Spectral synthesis method

Spectral synthesis methods rely on various integral transformations [26]. This approach enables direct operation on the spectral characteristics of the output signal. Methods utilizing the Fourier transform have gained significant popularity. The algorithm of this method in the one-dimensional case is considered as follows.

Initially, white noise with a normal distribution law is generated in the spatial domain of the required size.

DOI: 10.20535/2523-4455.mea.291803

Commonly, this involves using noise with zero mean and unit variance, also known as Gaussian noise. However, depending on specific requirements, these statistical parameters may vary.

Then, the noise spectrum is obtained using the Fourier transform:

$$R = F\left[r\right] = X + jY,$$

where X, Y – random variables with normal distribution.

Once the spectrum of white noise in the frequency domain is determined, a filtering function F is applied to achieve the desired PSD. Various functions can serve this purpose. To generate the cloud cover, a discrete version of the $1/f$ noise distribution law, as previously described, is utilized. Consequently, the following is obtained:

$$R^{'} = R \cdot F \qquad (2)$$

To find the original noise with the necessary spectral characteristics, the inverse Fourier transform is used:

$$r = F^{-1}\left[R^{'} \right]$$

An example of cloud cover obtained by two-dimensional spectral synthesis is shown in Fig. 1.

The isotropic nature of the resulting noise, attributed to the filter function being a rotation figure, poses a disadvantage in cloud cover modeling, as real cloud cover exhibits a certain degree of anisotropy. To address this limitation, modifications to the current spectral synthesis method are required.

C. *Mathematical model of anisotropic spectral synthesis*

For model development, an analysis of the spectral characteristics using a real image of cumulus cloud cover (Fig. 2) is required.

The Fourier transform presupposes the periodicity of the target function. However, the example cloud cover image (Fig. 2) is not periodic, resulting in a pronounced jump at the image boundaries. This discrepancy leads to spectrum leakage, significantly influencing the spectral characteristics [28].

To mitigate or reduce this effect, various window functions are employed [29]. For the two-dimensional case, window function is defined as:

$$W = \frac{1 - \sqrt{k_x^2 + k_y^2}}{\max\left(k_x^2 + k_y^2\right)},$$

where k_x – the number of the spectral component along the abscissa axis, k_y – the number of the spectral component along the ordinate axis.

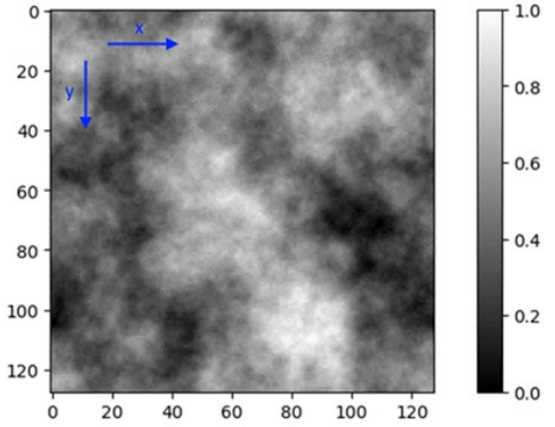

Fig. 1 An example of a cloud cover image obtained using two-dimensional spectral synthesis. Arrows determine the positive directions of the axes

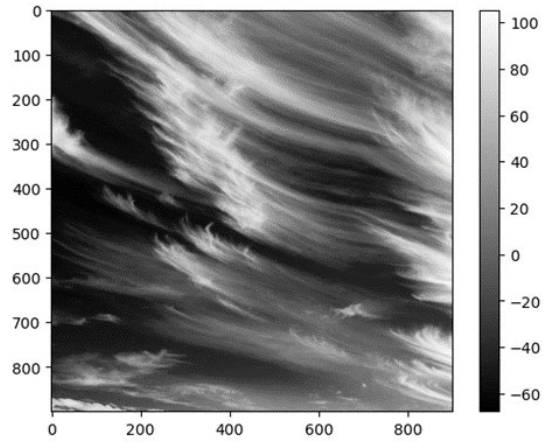

Fig. 2 Studied original image

The window function is applied to the original image, and the constant component of the original image is excluded to simplify the subsequent analysis of its spectral characteristics:

$$p_0 = W\left(p - \overline{p}\right),$$

where $\overline{p} = E\left[p\right]$ – mean value of examined image.

Upon the application of this window function, the appearance of the original image is as shown in Fig. 3. This application results in a visually smooth reduction in the brightness of the original image near its edges, effectively minimizing the impact of the spectrum leakage phenomenon.

The next step is to find the spectrum of the preprocessed image p_0 using the Fourier transform:

$$P = F\left[p_0\right] = X + jY$$

As well as magnitude and phase spectra (Fig. 4 and Fig. 5, a, respectively):

DOI: 10.20535/2523-4455.mea.291803

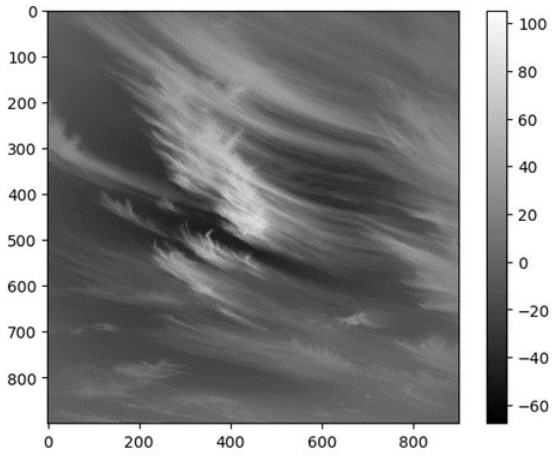

Fig. 3 Preprocessed studied image

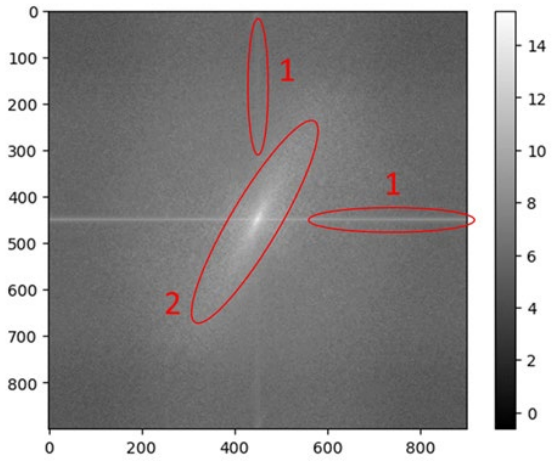

Fig. 4 Magnitude spectrum of windowed image: 1 – axial component, 2 – elliptical component

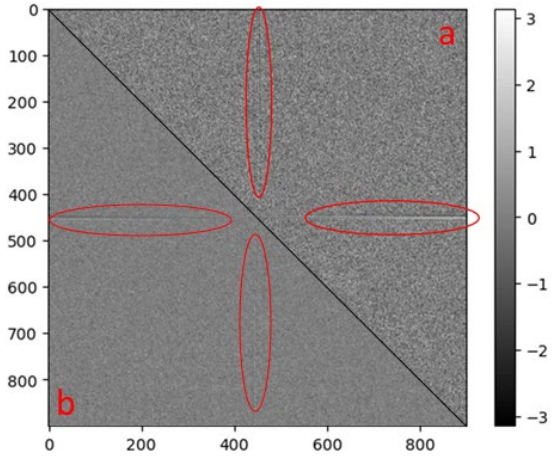

Fig. 5 Phase spectrum of windowed image (a) and generated phase spectrum (b). Axial components are emphasized with circles

$$A_P = |P| = |X + jY|$$

$$\varphi_P = \arg P = \arg(X + jY)$$

The magnitude and phase spectra display distinct characteristics, notably the sections along the axes and an elliptical component (Fig. 4 and Fig. 5, a). For the generation of cloud cover using spectral synthesis, these specific features of the spectral characteristics need to be replicated.

The analysis begins with the phase response and its components along the axes. Approximating the phase response presents a complex task, as the distribution law is not clearly established, in contrast to the amplitude response. Therefore, spectral synthesis is employed for generating the phase.

Initially, the spectrum of the phase response is determined using the Fourier transform:

$$\Phi = F[\varphi] = X + jY$$

Followed by its magnitude spectrum:

$$A_\Phi = |\Phi| = |X + jY| \quad (3)$$

The obtained magnitude spectrum (3) is then used as a filtering function in the spectral synthesis procedure previously described (2):

$$\varphi_{out} = F^{-1}[A_\Phi \cdot R], \quad (4)$$

where R represents the white noise spectrum.

The application of this approach yields an approximate phase response φ_{out} (Fig. 5, b), mirroring the features and distribution law of the original phase response (Fig. 5, a).

In generating the phase spectrum characteristics by this method, it is observed that boundary values may extend beyond the range of $[-\pi, \pi]$. Nonetheless, the normalization of the phase spectrum is unnecessary due to the periodicity of the basic's functions in the Fourier transform.

Using the generated phase spectrum φ_{out}, the original magnitude spectrum A_P, and the inverse Fourier transform, reconstructed image of the cloud cover can be defined as:

$$p = F^{-1}\left[A_P e^{j\varphi_{approx}} \right]$$

Upon analysis of the restored cloud cover image (Fig. 6), it is evident that the generated phase spectrum successfully captures most features of the research image of the cloud cover.

However, since this method of phase spectrum generation is pseudo-random, images produced using this phase will bear visual similarity to the original image. To address this limitation, a random phase spectrum can be defined as follows:

$$\varphi = \varepsilon\varphi_P + (1 - \varepsilon)\varphi_r, \quad (5)$$

DOI: 10.20535/2523-4455.mea.291803

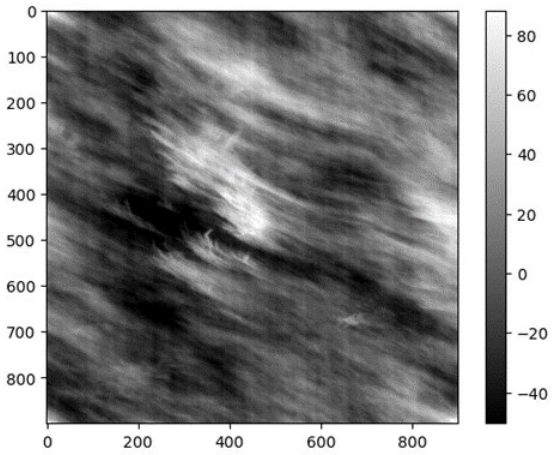

Fig. 6 Restored image using generated phase

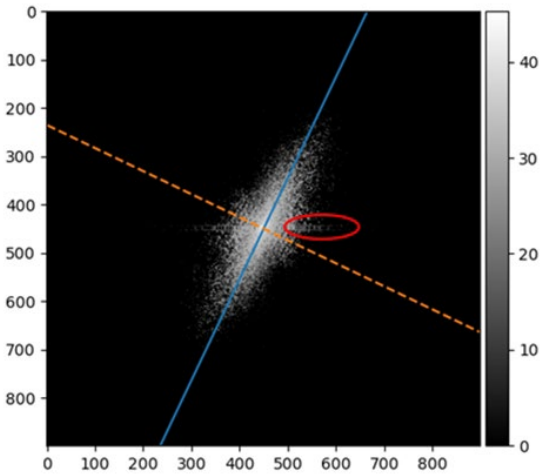

Fig. 7 Elliptical magnitude spectrum component. The solid line approximates the major axis of the ellipse, the dashed – minor axis. The red line shows the area of magnitude spectrum, where the components along the abscissa axis were replaced with the nearest neighboring

where φ_P – phase spectrum of the original image, φ_r – random phase spectrum, $\varepsilon = 0\ldots1$ – blending coefficient.

The subsequent step involves the approximation of the elliptical component of the magnitude spectrum. This requires determining the rotation angle of the elliptical component, as well as quantifying the attenuation along its major and minor semi-axes.

To determine the angle of rotation, it is necessary to select the elliptical component of the magnitude spectrum:

$$A_{el} = \begin{cases} A_P, A_P \geq th \\ 0, A_P < 0 \end{cases},$$

where th represents the threshold value corresponding to the boundaries of the elliptical component.

This threshold value is established experimentally, and for the magnitude spectrum of the analyzed image (Fig. 3) on a logarithmic scale it is equal to $th = 9$. Nonetheless, this approach does not allow for the complete separation of the elliptical component from the axial components, resulting in potential inaccuracies in determining the rotation angle. To mitigate this issue, sections of the spectrum that cannot be distinctly categorized are substituted with zero values or the nearest discernible components (either horizontal or vertical), emphasizing the presence of the elliptical component. Fig. 7 illustrates this process, with the relevant modifications highlighted in red.

After that, the angle of rotation is determined through linear regression. Additionally, a weighting function is implemented to augment the impact of low-frequency components on the regression outcome. In this context, the objective is to minimize the following difference using the least squares method:

$$SSE = \sum_i \sum_j A_{el}^2 \left(k_y - \hat{a} k_x \right), \tag{6}$$

where k_x, k_y – the number of the spectral component along the corresponding axis, A_{el} – elliptical component of the magnitude spectrum. It should be noted that all variables in equation (6) are dependent on i and j, although this dependency is omitted in the notation for simplicity.

For this purpose, the partial derivative with respect to the angular coefficient is calculated and then set to zero:

$$\frac{\partial}{\partial \hat{a}} SSE = -2 \sum_i \sum_j A_{el}^2 \left(k_y - \hat{a} k_x \right) k_x = 0 \tag{7}$$

Having solved the resulting equation for the desired parameter, a linear regression equation through the origin of coordinates is obtained [30], with the magnitude spectrum serving as a weighting function:

$$\hat{a} = \frac{\sum_i \sum_j A_{ellipcit}^2 k_y k_x}{\sum_i \sum_j A_{ellipcit}^2 k_x^2} = \frac{\langle k_y k_x \rangle}{\langle k_x^2 \rangle} \tag{8}$$

The average value in formula (8) is determined as follows:

$$\langle f(i,j) \rangle = \frac{\sum_i \sum_j A_{ellipcit}^2 f(i,j)}{\sum_i \sum_j A_{ellipcit}^2} \tag{9}$$

Regression analysis involves the presence of a dependent variable and one or more independent variables. Formula (8) assumes that is an independent variable, but experimentally it was established that

DOI: 10.20535/2523-4455.mea.291803

sometimes it is more appropriate to choose as an independent variable. In this case, equation (8) takes the form:

$$\hat{a} = \frac{\langle k_y k_x \rangle}{\langle k_y^2 \rangle} \tag{10}$$

The next step involves approximating the magnitude spectrum along the axes of the elliptical component. The PSD distribution law of the $1/f$ noise (1) is proposed as the approximating function. However, this approach necessitates determining two parameters: the attenuation coefficient α and the constant c. Employing the method of least squares in this context necessitates solving a system of two transcendental equations, which demands the application of numerical methods [31]. Such a requirement significantly complicates the algorithm and reduces its computational speed.

Therefore, for simplification, the magnitude spectrum normalization is performed as follows:

$$A_{Pn} = \frac{A_P}{\max(A_P)}$$

Using this approach allows you to significantly simplify the approximation process.

Next, employing the method of least squares results in an exponential regression scenario that simplifies to a linear case [32]:

$$SSE = \sum_i \left[\log A_{Pn} - \left(-\hat{\alpha} \log k\right) \right]^2 \tag{11}$$

By applying the approach used in equations (7)-(8) to equation (11), the following is obtained:

$$\hat{\alpha} = -\frac{\sum_i \log k \log A_{Pn}}{\sum_i \log^2 k} = -\frac{\langle \log k \log A_{Pn} \rangle}{\langle \log^2 k \rangle} \tag{12}$$

In turn, the following distribution function is used to approximate the magnitude spectrum:

$$A_{out} = \sqrt{(1-\eta)M^2 + \eta N^2}, \tag{13}$$

where $\eta = 1 - \alpha_{min}/\alpha_{maj}$ – blending coefficient which determines the degree of stretching of the symmetric distribution law $M = 1/x^{\alpha_{minor}}$ along line $N = k_y - \alpha_{maj} k_x$, α_{maj}, α_{min} – attenuation coefficient along the major and minor axes respectively.

It was also experimentally established that the linear components of the magnitude spectrum along the axes are quite difficult to approximate, and their influence on the generated images is quite small, so they can be neglected.

Thus, to generate images of cloud cover of a certain type, it is necessary to find four parameters: the attenuation coefficient along the major α_{maj} and minor α_{min} axes of the elliptical components of magnitude spectrum, the angle of rotation a of the elliptical component, and the phase spectrum φ (original or pseudorandom). That is, the developed cloud cover model contains four parameters.

D. *Algorithm for finding the parameters of the developed model*

The flowchart of the algorithm for finding the parameters of the developed model is shown in Fig. 8.

Cloud cover images of a specific type serve as the input data. In scenarios involving multiple images, the algorithm is applied to each image individually. Subsequently, the parameters determined from each image are averaged. Based on these averaged parameters, the output image is then generated.

In the process of approximating the magnitude spectrum, as exemplified in equations (8) and (10), a change in the signal energy occurs. This alteration can result in a notable discrepancy in values between the original set of images and the generated image. To counteract this issue, normalization is required. This involves the use of a proportionality factor, which quantifies the ratio by which the energy of the original image exceeds that of the generated image:

$$c_{PSD} = \sqrt{\frac{\sum_{i,j} A_{out}^2(i,j)}{\sum_{i,j} A_P^2(i,j)}},$$

where A_{out} – magnitude spectrum of generated image, A_P – magnitude spectrum of the source image or the average magnitude spectrum of a set of input images.

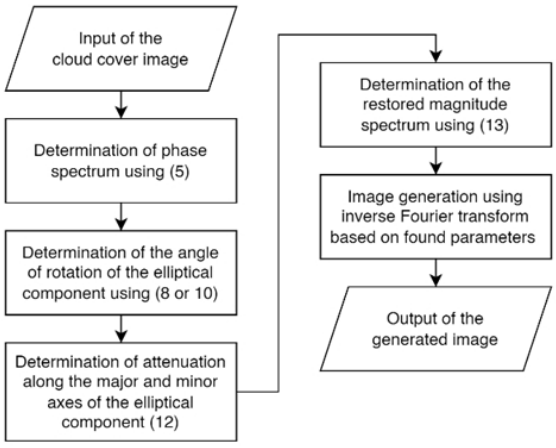

Fig. 8 Flowchart of the proposed method

DOI: 10.20535/2523-4455.mea.291803

Moreover, when employing a random phase at values $\varepsilon \approx 0$ in equation (5), there are instances where the value of proportionality $c_{PSD} \approx 1$, indicating that the energies of the output and generated signals are equivalent. Nonetheless, this can result in the presence of areas in the generated image that exceed the value range of the original image.

To align the generated image within the value range of the original image, linear regression is utilized [32]:

$$\hat{a} = \frac{\langle A_{approx} A_P \rangle - \langle A_{approx} \rangle \langle A_P \rangle}{\langle A_P^2 \rangle - \langle A_P \rangle^2}$$

$$\hat{b} = \langle A_P \rangle - \hat{a} \langle A_{approx} \rangle$$

Thus, the normalized magnitude spectrum is determined as follows:

$$A'_{approx} = \hat{a} c_{PSD} A_{approx} + \hat{b} \qquad (14)$$

In addition, after generating the cloud cover image, using (14), it is necessary to bring the image to the range of the original image:

$$R'_{outp} = \begin{cases} R_{outp}, \ \min(R_{inp}) \le R_{outp} \le \max(R_{inp}) \\ \min(R_{inp}), \ R_{outp} \le \min(R_{inp}) \\ \max(R_{inp}), \ R_{outp} \ge \max(R_{inp}) \end{cases}$$

Furthermore, experimental findings indicate that in cases where long tails are present along one of the frequency response axes, it is recommended to consider this variable as the dependent variable in determining the magnitude spectrum rotation angle $\hat{a}$, utilizing the appropriate formula – either (8) or (10). For instance, in the magnitude spectrum of the studied image (Fig. 4), tails are observed along the x axis, thus making the use of formula (10) more suitable. Employing formula (8) in such scenarios could result in an inaccurate estimation of the rotation angle.

III. Results and Discussion

To validate the developed method of spectral synthesis, a comparative analysis was conducted against the traditional method of spectral synthesis, focusing on the accuracy of approximating the original image.

In both approaches, the phase spectrum of the original image was employed. In the traditional method, the frequency response is determined using equation (13), under the assumption of symmetry, i.e. $\eta = 0$.

The accuracy of the approximation is estimated using the root mean square error:

$$RMSE = \sqrt{\frac{1}{mn} \sum_{i=1}^{n} \sum_{j=1}^{m} \left[P(i,j) - P'(i,j) \right]^2},$$

where $P(i,j)$ – pixel value of the original image with coordinates (i,j), $P'(i,j)$ – pixel value of the generated image with coordinates (i,j)

The results obtained from applying the proposed algorithm (Fig. 8) and the traditional approach to the analyzed image are displayed in Table 1. Images restored using these methods are illustrated in Fig. 9 and Fig. 10.

Table 1 Approximation parameters of the original cloud cover image

	Proposed method	Basic approach
α_{maj}	1,447	-
α_{min}	1,591	1,572
a	-2,095	-
η	0,0996	-
RMSE	22,956	28,982

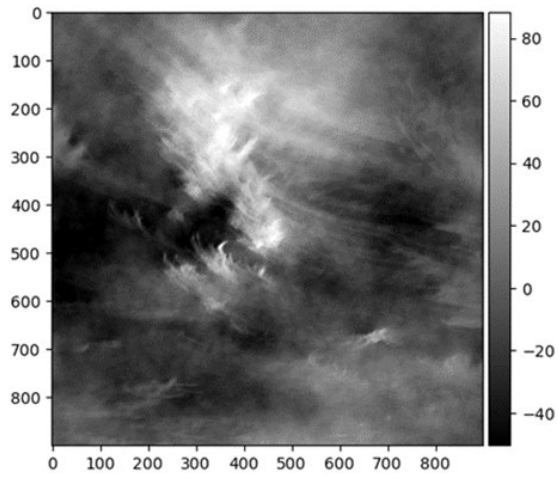

Fig. 9 Recovered images using a traditional spectral synthesis approach

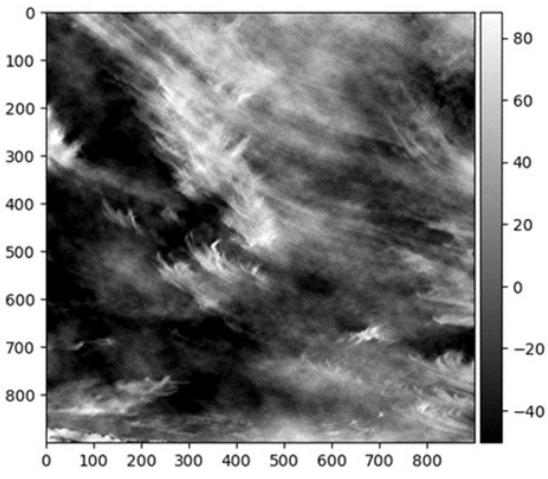

Fig. 10 Recovered images using proposed method

DOI: 10.20535/2523-4455.mea.291803

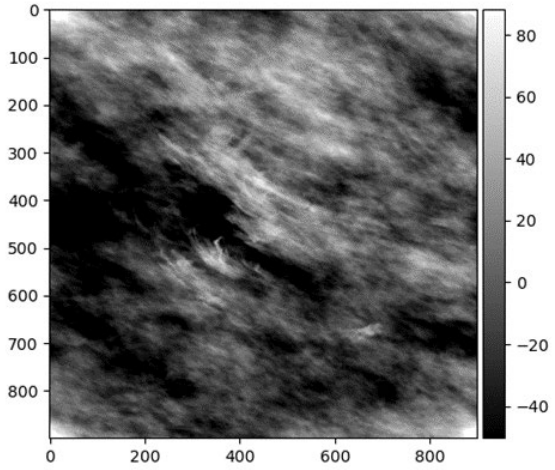

Fig. 11 Pseudo-random image generated using proposed method with $\varepsilon = 0.4$

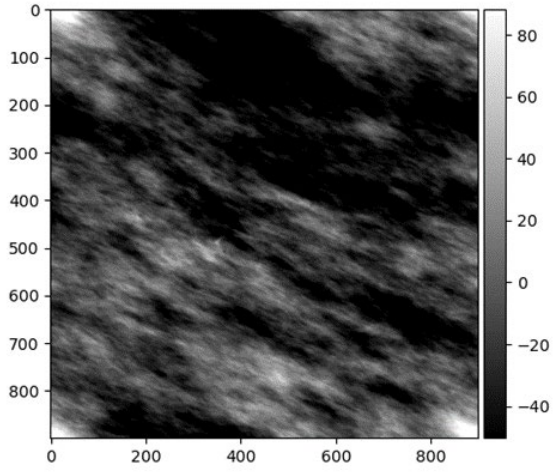

Fig. 12 Pseudo-random image generated using proposed method with $\varepsilon = 0.6$

Table 1 demonstrates that the proposed method yields a 20.79% lower image approximation error for the studied image compared to the traditional method. Both methods yield similar values for the attenuation coefficient α_{min}.

In the analysis of the generated images (Fig. 9 and Fig. 10), it is evident that the image produced using the proposed method visually is more similar to the original image (Fig. 2). The traditional method, characterized by an isotropic magnitude spectrum with an attenuation coefficient α_{min}, leads to a reduction in the amplitude of harmonics along the elliptical component's semimajor axis, resulting in a loss of detail in the traditionally generated image.

Additionally, examples of the proposed method in producing pseudo-random cloud cover images is demonstrated, employing a range of values of $\varepsilon = 0{,}4$ (Fig. 11) and $\varepsilon = 0{,}6$ (Fig. 12) in the equation (5). While the quality of these images may be lower compared to the recovered image (Fig. 10), they serve the purpose of generating pseudo-random cloud cover that closely mimics the spectral parameters of the input image.

The images generated through this method successfully retain key characteristics of the original, such as the direction and length of low-frequency components. The values of $\eta < 0{,}5$ effectively maintain the phase information of the high-frequency components of the original image, sustaining the detail in the generated images. While, values $\eta \geq 0{,}5$ lead to a dominance of the random component in the phase spectrum, facilitating the creation of pseudo-random images.

Conclusions

In this study, a new mathematical model for creating images of cloud covers has been developed. This model is particularly beneficial for studying how cloud shadows affect solar panels, known as PV partial shading. The focus was on achieving images that closely match real cloud patterns.

The main achievement of this work is the accurate replication of cloud appearance and behavior. This is crucial for understanding the impact of cloud-induced shadows on solar panels, influencing their energy output.

The significance of this research extends beyond just producing cloud images; it plays a vital role in solar energy advancement. The model allows for better planning and management of solar panel systems, particularly in areas with variable sunlight due to cloud cover.

Looking forward, this model could be integrated into systems predicting solar panel energy output, enhancing the reliability and efficiency of solar power.

In essence, this study represents a significant advancement in producing accurate cloud images and contributes substantially to optimizing solar panel performance under varied cloud conditions.

Comparative analysis indicates that the proposed cloud cover image synthesis method yields, on average, a 20% lower approximation error relative to the traditional spectral synthesis approach. Visually, this translates to a greater resemblance to the original cloud cover image.

DOI: 10.20535/2523-4455.mea.291803

References

[1] H. Ritchie, M. Roser, and P. Rosado, "Energy," Our World Data, Oct. 2022, **URL:** https://ourworldindata.org/energy.

[2] T. Y. Gnangoin, D. F. Kassi, A. J.-R. Edjoukou, O. Kongrong, and D. Yuqing, "Renewable energy, non-renewable energy, economic growth and CO2 emissions in the newly emerging market economies: The moderating role of human capital," Front. Environ. Sci., vol. 10, Sep. 2022, **DOI:** 10.3389/fenvs.2022.1017721.

[3] D. Gielen, F. Boshell, D. Saygin, M. D. Bazilian, N. Wagner, and R. Gorini, "The role of renewable energy in the global energy transformation," Energy Strateg. Rev., vol. 24, pp. 38–50, Apr. 2019, **DOI:** 10.1016/j.esr.2019.01.006.

[4] "Electricity Market Report 2023 – Analysis - IEA." [Online]. Available: https://www.iea.org/reports/electricity-market-report-2023. [Accessed: 27-Sep-2023].

[5] O. Diachuk, M. Chepeliev, R. Podolets, H. Trypolska, V. Venher, T. Saprykina and R. Yukhymets *"Perekhid Ukrayiny na vidnovlyuvanu enerhetyku do 2050 r. [Transition of Ukraine to renewable energy until 2050.]"* Heinrich Böll Stiftung : Kyiv, Ukraine, 2023 [Online]. Available: https://ua.boell.org/sites/default/files/perehid_ukraini_na_vidnovlyuvanu_energetiku_do_2050_roku.pdf [Accessed: 27-Sep-2023].

[6] D. Maradin, "ADVANTAGES AND DISADVANTAGES OF RENEWABLE ENERGY SOURCES UTILIZATION," Int. J. Energy Econ. Policy, vol. 11, no. 3, pp. 176–183, Apr. 2021, **DOI:** 10.32479/ijeep.11027.

[7] V. M. Geyets, O. V. Kirilenko, B. I. Basok, and Y. T. Baseyev, "Energy Strategy: Projections (Review)," Nauk. ta innovacii, vol. 16, no. 1, pp. 3–15, 2020, **DOI:** 10.15407/scin16.01.003.

[8] I. R. E. A. (IRENA), "REmap 2030, Renewable Energy Prospects: Ukraine, a background paper." IRENA: International Renewable Energy Agency, 13-Apr-2015.

[9] "Ukraine energy profile – Analysis - IEA." [Online]. Available: https://www.iea.org/reports/ukraine-energy-profile. [Accessed: 27-Sep-2023].

[10] K. Sopian, S. L. Cheow, and S. H. Zaidi, "An overview of crystalline silicon solar cell technology: Past, present, and future," 2017, p. 020004, **DOI:** 10.1063/1.4999854.

[11] D. O. Akinyele, R. K. Rayudu, and N. K. C. Nair, "Global progress in photovoltaic technologies and the scenario of development of solar panel plant and module performance estimation – Application in Nigeria," Renew. Sustain. Energy Rev., vol. 48, pp. 112–139, Aug. 2015, **DOI:** 10.1016/j.rser.2015.03.021.

[12] J. Teo, R. Tan, V. Mok, V. Ramachandaramurthy, and C. Tan, "Impact of Partial Shading on the P-V Characteristics and the Maximum Power of a Photovoltaic String," Energies, vol. 11, no. 7, p. 1860, Jul. 2018, **DOI:** 10.3390/en11071860.

[13] E. J. Wolf, I. E. Gould, L. B. Bliss, J. J. Berry, and M. D. McGehee, "Designing Modules to Prevent Reverse Bias Degradation in Perovskite Solar Cells when Partial Shading Occurs," Sol. RRL, vol. 6, no. 3, Mar. 2022, **DOI:** 10.1002/solr.202100239.

[14] M. A. Al Mamun, M. Hasanuzzaman, and J. Selvaraj, "Experimental investigation of the effect of partial shading on photovoltaic performance," IET Renew. Power Gener., vol. 11, no. 7, pp. 912–921, Jun. 2017, **DOI:** 10.1049/iet-rpg.2016.0902.

[15] A. M. Ajmal, T. Sudhakar Babu, V. K. Ramachandaramurthy, D. Yousri, and J. B. Ekanayake, "Static and dynamic reconfiguration approaches for mitigation of partial shading influence in photovoltaic arrays," Sustain. Energy Technol. Assessments, vol. 40, p. 100738, Aug. 2020, **DOI:** 10.1016/j.seta.2020.100738.

[16] Y. J. Kaufman, "Aerosol optical thickness and atmospheric path radiance," J. Geophys. Res. Atmos., vol. 98, no. D2, pp. 2677–2692, Feb. 1993, **DOI:** 10.1029/92JD02427.

[17] M. Chin et al., "Tropospheric Aerosol Optical Thickness from the GOCART Model and Comparisons with Satellite and Sun Photometer Measurements," J. Atmos. Sci., vol. 59, no. 3, pp. 461–483, Feb. 2002, **DOI:** 10.1175/1520-0469(2002)059<0461:TAOTFT>2.0.CO;2.

[18] M. Bradley and M. Gasseller, "Measurement of Aerosols Optical Thickness of the Atmosphere using the GLOBE Handheld Sun Photometer," J. Vis. Exp., no. 147, May 2019, **DOI:** 10.3791/59257.

[19] S. Kato et al., "A comparison of the aerosol thickness derived from ground-based and airborne measurements," J. Geophys. Res. Atmos., vol. 105, no. D11, pp. 14701–14717, Jun. 2000, **DOI:** 10.1029/2000JD900013.

[20] D. R. Myers, "Solar Radiation Resource Assessment for Renewable Energy Conversion," in Comprehensive Renewable Energy, Elsevier, 2012, pp. 213–237, **DOI:** 10.1016/B978-0-08-087872-0.00112-8.

[21] D. Serrano, M. J. Marín, M. Núñez, S. Gandía, M. P. Utrillas, and J. A. Martínez-Lozano, "Relationship between the effective cloud optical depth and different atmospheric transmission factors," Atmos. Res., vol. 160, pp. 50–58, Jun. 2015, **DOI:** 10.1016/j.atmosres.2015.03.004.

[22] P. Bak, C. Tang, and K. Wiesenfeld, "Self-organized criticality: An explanation of the 1/ f noise," Phys. Rev. Lett., vol. 59, no. 4, pp. 381–384, Jul. 1987, **DOI:** 10.1103/PhysRevLett.59.381.

[23] F. N. Hooge, T. G. M. Kleinpenning, and L. K. J. Vandamme, "Experimental studies on 1/f noise," Reports Prog. Phys., vol. 44, no. 5, pp. 479–532, May 1981, **DOI:** 10.1088/0034-4885/44/5/001.

[24] D. L. Gilden, T. Thornton, and M. W. Mallon, "1/ f Noise in Human Cognition," Science (80-.)., vol. 267, no. 5205, pp. 1837–1839, Mar. 1995, **DOI:** 10.1126/science.7892611.

[25] B. Kaulakys and T. Meškauskas, "Modeling 1/f noise," Phys. Rev. E, vol. 58, no. 6, pp. 7013–7019, Dec. 1998, **DOI:** 10.1103/PhysRevE.58.7013.

[26] A. Lagae, S. Lefebvre, R. Cook, T. DeRose, G. Drettakis, D. S. Ebert, J. P. Lewis, K. Perlin and M. Zwicker, "State of the Art in Procedural Noise Functions," The Eurographics Association 200x, 2010.
URL: https://www-sop.inria.fr/reves/Basilic/2010/LLCDDELPZ10/LLCDDELPZ10STARPNF.pdf.

[27] A. Goldberg, M. Zwicker, and F. Durand, "Anisotropic noise," ACM Trans. Graph., vol. 27, no. 3, pp. 1–8, Aug. 2008, **DOI:** 10.1145/1360612.1360653.

[28] D. Lyon, “The Discrete Fourier Transform, Part 4: Spectral Leakage.,” J. Object Technol., vol. 8, no. 7, p. 23, 2009, **DOI:** 10.5381/jot.2009.8.7.c2.

[29] D.-J. Jwo, W.-Y. Chang, and I.-H. Wu, “Windowing Techniques, the Welch Method for Improvement of Power Spectrum Estimation,” Comput. Mater. Contin., vol. 67, no. 3, pp. 3983–4003, 2021, **DOI:** 10.32604/cmc.2021.014752.

[30] J. G. Eisenhauer, “Regression through the Origin,” Teach. Stat., vol. 25, no. 3, pp. 76–80, 2003, **DOI:** 10.1111/1467-9639.00136.

[31] S. Kaur and S. K. Sharma, “An Efficient Iterative Methods for Solving Transcendental Equations,” 2023, pp. 191–203, **DOI:** 10.1007/978-981-99-2468-4_15.

[32] M. Kutner, C. Nachtsheim, and J. Neter, Applied Linear Regression Models- 4th Edition with Student CD (McGraw Hill/Irwin Series: Operations and Decision Sciences), 4th ed. McGraw Hill, 2004, **ISBN:** 978-0073014661.

Надійшла до редакції 29 листопада 2023 року
Прийнята до друку 26 грудня 2023 року

DOI: 10.20535/2523-4455.mea.291803

УДК 621.314

Генерація анізотропного хмарного покриву

В. І. Мартинюк[f], 0000-0003-0882-5114
В. Я. Жуйков[s], 0000-0002-3338-2426
Національний технічний університет України
«Київський політехнічний інститут імені Ігоря Сікорського» 00syn5v21
Київ, Україна

Анотація*—У цій статті представлено розробку математичної моделі для генерації та аналізу зображень хмарного покриву, спеціально призначеної для покращення дослідження часткового затінення фотоелектричних систем. Розробка моделі включала ретельний аналіз реальних зображень хмарного покриву, з особливим акцентом на відтворення їх анізотропних спектральних характеристик за допомогою комбінації спектрального аналізу та різноманітних методів обробки зображень. Методологічно дослідження було зосереджено на розробці моделі з чотирма параметрами для точного відображення спектральних властивостей хмарного покриву. Основні параметри були визначені за допомогою використання різноманітних моделей регресійного аналізу, щоб відповідати характеристикам реальних хмар. Це включало аналіз амплітудних та фазових спектрів хмарних покривів та їхню адаптацію до моделі, здатної точно відтворювати ці властивості. Важливою частиною дослідження було формування нової техніки генерації фазового спектру. Ця техніка була розроблена для контролю ступеня схожості між згенерованим та оригінальними зображеннями, що забезпечує ефективність моделі в різних сценаріях моделювання хмарного покриву. Точність моделі у відтворенні характеристик хмарного покриву була перевірена порівняльним аналізом із традиційними методами спектральної синтезу. Цей аналіз включав генерацію зображень хмарного покриву за допомогою розробленої моделі та порівняння цих зображень із оригінальними хмарами за візуальною схожістю та похибкою апроксимації. Було встановлено, що розроблена модель у порівнянні з традиційним підходом спектрального синтезу забезпечує в середньому на 20% меншу похибку апроксимації вихідного зображення. Візуально це відображається у більшій чіткості згенерованого зображення хмарного покриву. Окрім того, модель була застосована для генерації псевдовипадкових зображень хмарного покриву шляхом зміни значення параметру моделі, який відповідає за анізотропію амплітудного спектру. Це дозволяє генерувати зображення, які одночасно є випадковими та відповідають спектральним характеристикам вихідного зображення хмарного покриву, зберігаючи ключові особливості, такі як напрямок, довжина та щільність. У підсумку, ця стаття детально описує створення високоточної моделі синтезу зображень хмарного покриву, з акцентом на точності спектральних властивостей. Дослідження підкреслює використання передових методів спектрального аналізу та обробки зображень для визначення ключових параметрів моделі, що призвело до значного прогресу в імітації хмарного покриву для сонячної енергетики.

Ключові слова — спектральний синтез; часткове затінення; моделювання хмарного покриву; точність апроксимації зображення; спектральна анізотропія; аналіз частотної характеристики; генерація фазового спектру